18. MAGNETIC PROPERTIES OF BASEMENT ROCK SAMPLES FROM CATOCHE KNOLL, GULF OF MEXICO, DEEP SEA DRILLING PROJECT LEG 77[1]

Toshio Furuta, Ocean Research Institute, University of Tokyo, Nakano, Tokyo 164, Japan
and
Hajimu Kinoshita, Faculty of Science, Chiba University, Yayoi, Chiba 280, Japan

ABSTRACT

Magnetic properties of doleritic and some metamorphic basement rocks underlying Catoche Knoll are studied. Doleritic rocks show a high saturation magnetic moment (2–5 emu/g) compared to metamorphic rocks (0.1–1 emu/g). Magnetic minerals of rocks from this hole show a high stability when heated in vacuo up to 600°C at a fixed rate of heating. Curie temperatures are distributed close to 550°C. These properties differ markedly from those of common submarine basalts observed before. X-ray microprobe analysis techniques were used to determine internal structures of ferromagnetic minerals; in most of ferromagnetic minerals there exist two different types of magnetic phases (i.e., products of high-temperature and low-temperature oxidations). Interpretations on the coexisting, seemingly contradictory, phases can be made based upon present analyses.

INTRODUCTION

Rock magnetic studies of basement rocks of the ocean floor provide an important viewpoint for understanding the paleomagnetic structures and origin of the basement layers. Hole 538A (Fig. 1) has given us an opportunity to examine rock samples from a metamorphic gneiss and doleritic rocks that are overlain by the gneiss and by sediments. The crust beneath Hole 538A (Catoche Knoll; 23°50.95′N, 85°09.93′, Gulf of Mexico) is considered to be transitional between continental crust and oceanic crust. The sedimentary rocks directly overlying the basement complex at this site are late Albian to early Berriasian in age (~135 Ma).

Magnetic properties of 37 rock samples recovered from Hole 538A were examined. Natural remanent magnetization (Jn), saturation magnetization (Js), and temperature dependence of Js (Js-T) were measured. In addition, the internal microscopic structures of the ferromagnetic constituents in rock samples were observed over the surface of polished thin sections by reflection light microscopy and X-ray microprobe analysis. It will be made clear through the present study that (1) doleritic rocks of this site suffered from a certain grade of oxidation at high temperature as evidenced by exsolution lamellae, (2) low-temperature oxidation (maghemitization of titanomagnetite) is observable, (3) the ferromagnetic component is stable when heated up to 600°C in vacuo (10^{-4} Pa), and (4) the dolerite mass has magnetic properties that are similar to those of continental basaltic rocks.

RESULTS AND DISCUSSION

Saturation Magnetization and Susceptibility

Saturation magnetization values (Js) of rock samples from this hole are listed in Appendix A. Generally speaking, the saturation magnetization of doleritic rocks of this hole are higher than those of other doleritic samples obtained by DSDP so far. The variation of the Js of the samples downhole may reflect the chemical compositional variation and/or the amount of ferromagnetic constituents of the body. Samples taken from the metamorphic body show Js markedly lower than that of dolerites. The intensity of the natural remanent magnetization (Jn) and the susceptibility (K) show a similar tendency (i.e., higher values for dolerite and lower values for metamorphic rock samples). This feature may safely be explained as a reflection of the difference in their ferromagnetic mineral abundances.

Thermomagnetic Analysis

METHODS

We used a thermomagnetic balance to measure the temperature dependence of the saturation magnetization (Js = T) of all samples. A small fragment (~100 mg) of rock was chipped off the samples and placed between a pair of magnetic poles that induce a high magnetic field (4.5 kOe) around the sample space. The system is evacuated down to 10^{-3} to 10^{-4} Pa (~10^{-5} to 10^{-6} torr) and the sample is then heated and cooled at fixed rates (temperature change, 6°C/minute). Samples were kept at the maximum experimental temperature (650°C) for about 10 minutes during each run. Several samples were heated up to 725°C to test for a hematite component.

Results

Two significantly different types of Js-T curves were obtained. One group of Js-T curves are characterized by (1) high Js values, (2) Curie temperatures around 550°C, (3) nearly reversible behavior, and (4) little contamination of paramagnetic components (Fig. 2A). The other group is represented by (1) lower Js values, (2) Curie temperature around 550°C, (3) slightly but clearly irreversible behavior, and (4) a large portion of paramagnetic components (Fig. 2B). The former group is typical for the doleritic rocks and the latter is characteristic for the metamorphic rocks from this hole. The parameters in relation to the Js-T measurements on the rock samples of this site are listed in Appendix A.

[1] Buffler, R. T., Schlager, W., et al., *Init. Repts. DSDP*, 77: Washington (U.S. Govt. Printing Office).

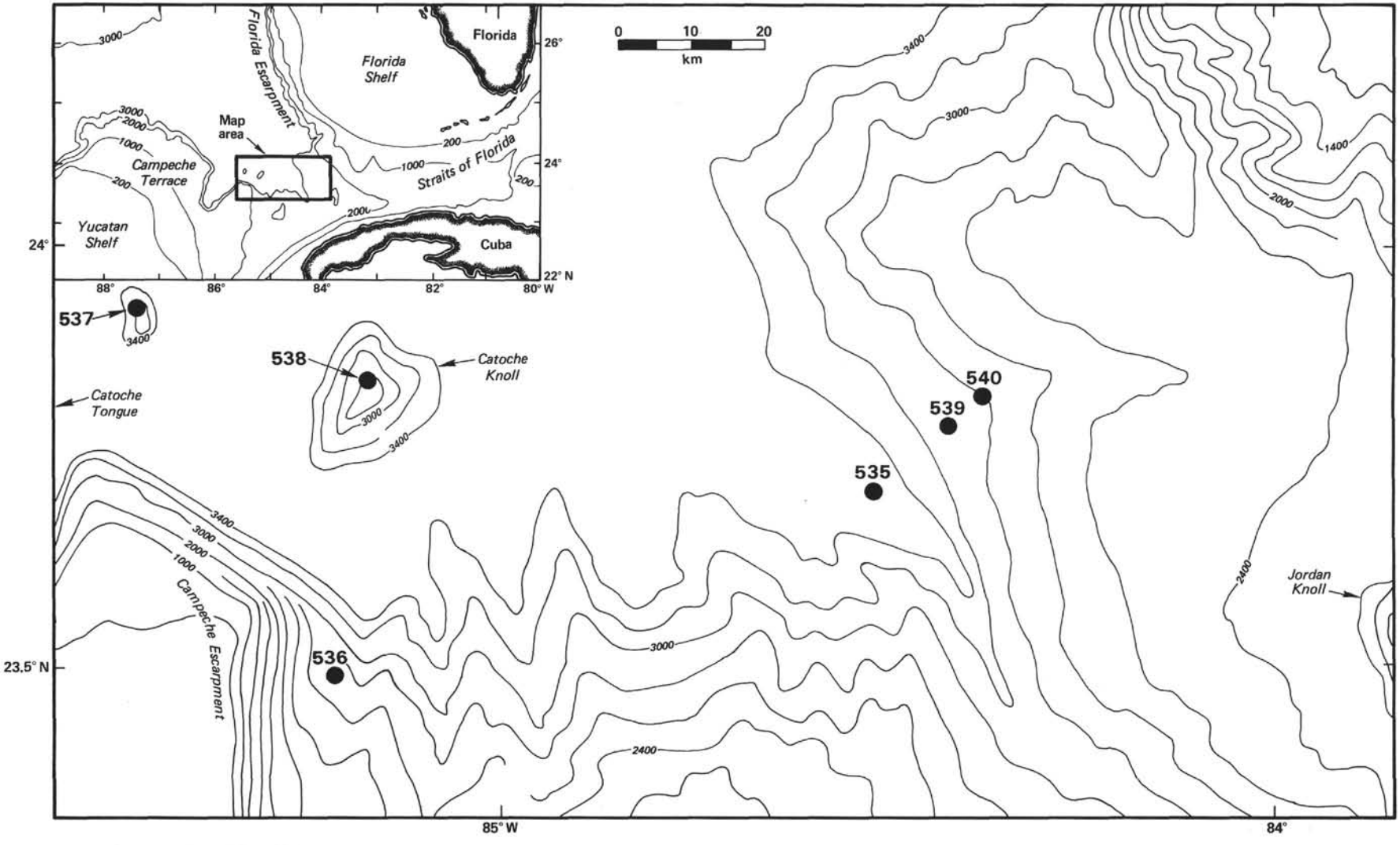

Figure 1. Location map, DSDP Leg 77 sites.

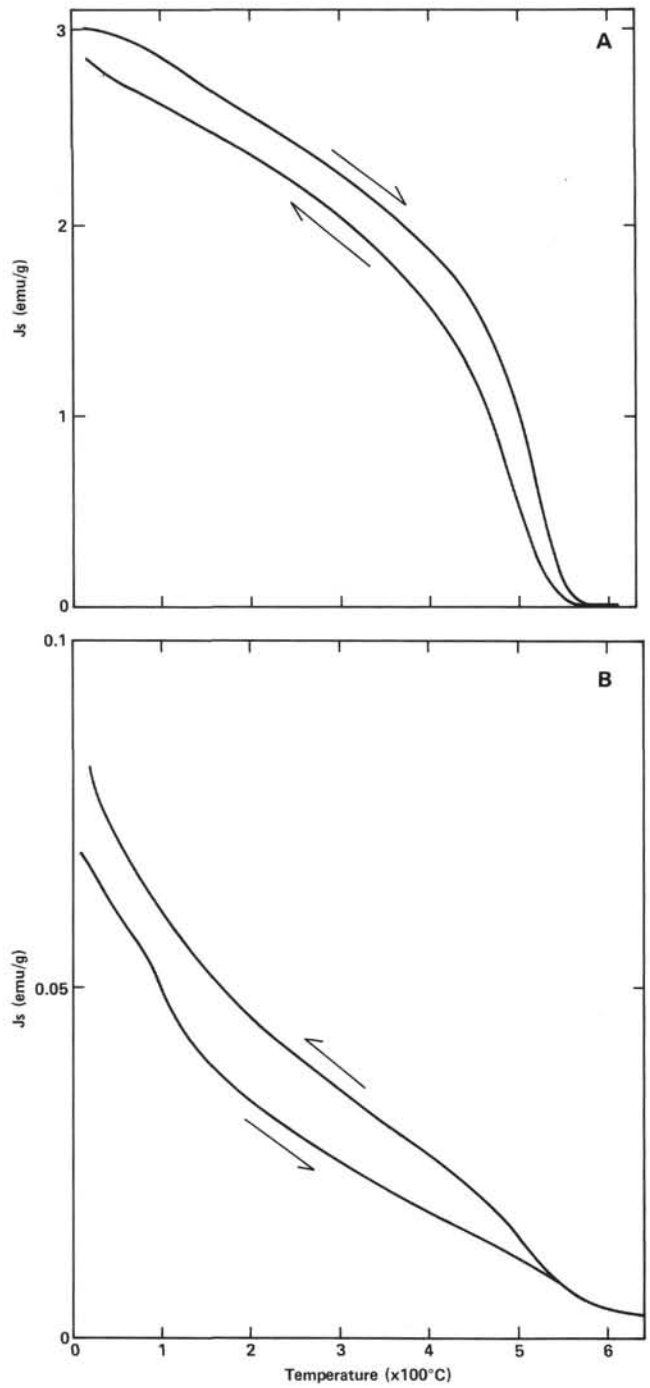

Figure 2. Thermomagnetic curves of typical samples. A. Thermally reversible with high Js (538A-32-1, 119–121 cm). B. Thermally irreversible with Js lower than Js of Figure 2A sample (538A-31-2, 47–50 cm).

Js-T analyses show that the temperature dependence of magnetic characteristics of ferromagnetic components of these basement rocks is clearly different from magnetic properties of submarine basaltic rocks, which commonly contain titanium-rich magnetite and show irreversible thermomagnetic behavior when heated beyond a certain temperature.

Microprobe Analysis of Opaque Minerals

METHODS

Contents of metallic ions (i.e., titanium and iron) were determined by means of electron probe microanalyzer (JXA-733; Japan Electro-Optical Laboratory). Several representative portions of titanomagnetite crystals were predetermined by an optical microscope before analyses. The electron beam was focused on a spot so that only a seemingly homogeneous area of the crystal under microscope was covered. However, in some cases when we found very fine internal structures (with the wavelength less than 1 μm), the radius of focus was not limited within homogeneous area and, therefore, defocused. In many cases in which the grain represented a series of relatively wide exsolution lamellae and/or large patches of secondary alteration products (probably of maghemite composition), contents of metallic ions were determined with high accuracy. The locations on the titanomagnetite crystals where the microprobe analyses were performed are shown in Figures 3–5.

Results

Some representative results of analyses for 26 spots on three typical rock samples in which we could find good grains with large diameter (60–100 μm) are listed in Appendix B. The main part of the titanomagnetite grains consists of titanium-poor titanomagnetite with x values of less than 0.2 [$x = x\mathrm{Fe_2TiO_4} \cdot (1 - x)\mathrm{Fe_3O_4}$]. The results of X-ray probe analyses of individual grains are briefly described below.

In Samples 538A-32-1, 119–121 cm, three spots in a titanomagnetite grain were scanned revealing significantly different Ti to Fe ratios. The first spot showed the Ti/Fe ratio close to 0.3; its value is somewhat similar to normal submarine basalts (Fig. 3B, Analysis Point 6). The second spot showed the Ti/Fe ratio around 0.1 (Analysis Points 3, 5, and 8, Fig. 3B–C and Appendix B), and the third one showed the ratio less than 0.006 (Analysis Points 1 and 2, Fig. 3B and Appendix B). The difference could have resulted from the high-temperature oxidation through which the Ti^{+4} ions were consumed by the production of ilmenite exsolution lamellae. The exsolution lamellae were identified as hemo-ilmenites and their Ti/Fe ratio varies between 0.81 and 0.88. By the backscattering electron image, the lamellae are less bright than the surrounding masses, which are composed of either titanomagnetite or titanomaghemite as shown in Figure 3A.

Analysis Point 6 in Figure 3B is selected in the middle of very fine ripple-type structure. The beam was defocused to a diameter of 20 microns, several times larger than usual, and the analysis was done over the whole area because the beam could not focus less than 1 micron and these fine structures could not be measured precisely. Total content of cations (mainly Ti and Fe) obtained from this arabesque texture is about 2% less than that of homogeneous titanomagnetite part. In contrast, the silica content of this area is large to some extent. The phenomenon (i.e., higher silica content and lower Ti and Fe cation content) is not an apparent effect of the defocusing but could be explained by an interdiffusion between silica glass and titanomagnetite phase. Fine structure around Analysis Point 4 (Fig. 3B) shows clearly an existence of very fine ilmeno-hematite lamel-

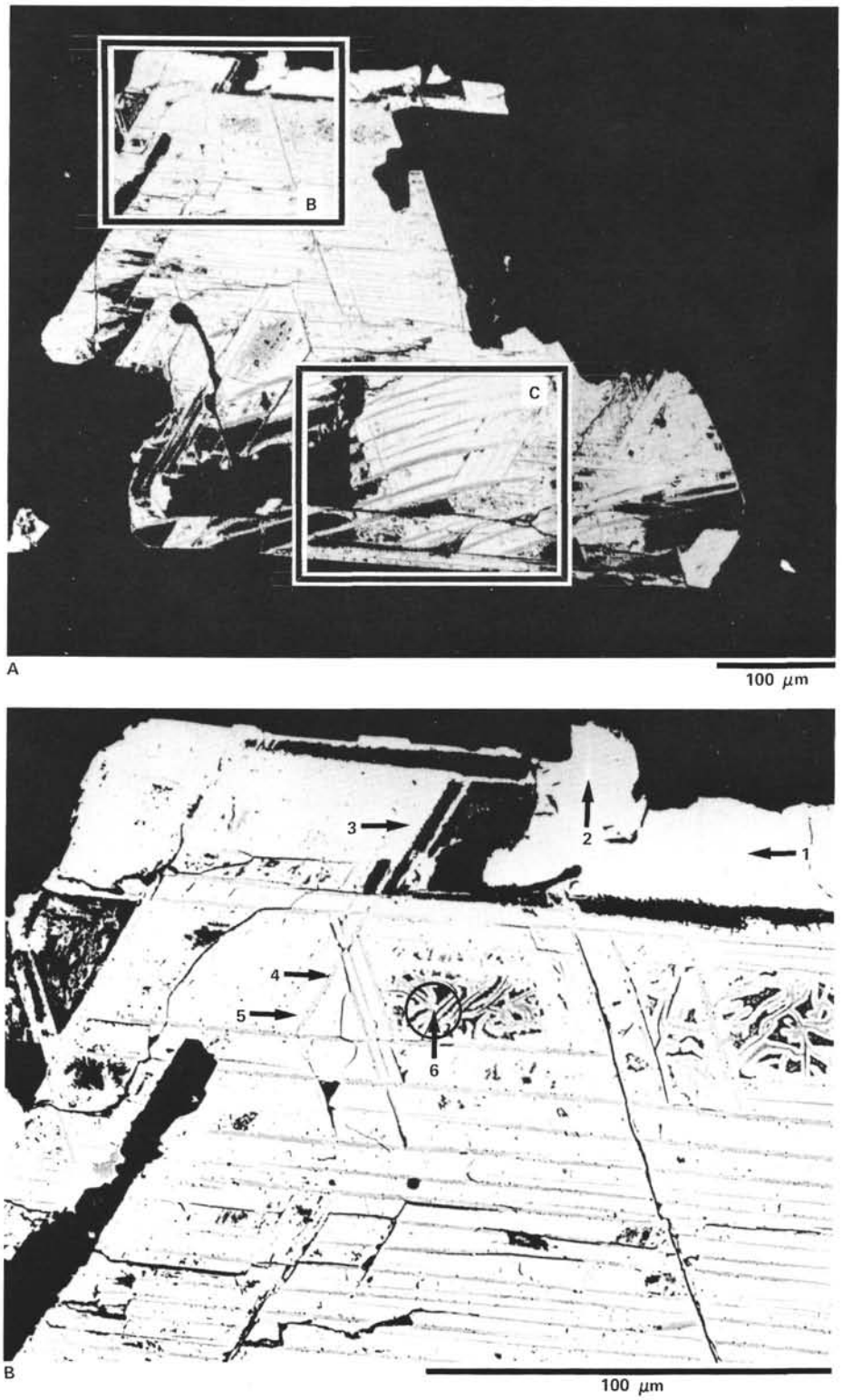

Figure 3. Microphotographs of electron compositional scanning image. The numbered arrows indicate analysis points (see Appendix B). A. Sample 538A-32-1, 119–121 cm; parts enclosed by squares labeled B and C correspond to Figures 3B and 3C, respectively. B. Enlarged part of Figure 3A; bright area consists of titanium-poor titanomagnetites (Analysis Points 1, 2, 3, and 5); gray thin lamellae are ilmenohematite (Analysis Point 4). The part with arabesque structure (Analysis Point 6) has a secondary texture caused by low-temperature oxidation that was analyzed with a defocused beam. C. Enlarged part of Figure 3A; bright area consists of titanomagnetite of moderate titanium content (Analysis Point 8). Thick lamellae are hemo-ilmenites (Analysis Points 7, 9, and 10). The skeletal texture between lamellae could result from maghemitization at high temperatures.

Figure 3. (Continued).

lae, and in these lamellae the Ti/Fe ratio is 0.3 (Appendix B, Analysis Point 4).

Sample 538A-32-6, 77–79 cm (Fig. 4) shows a series of exsolution lamellae and clusters of microcracks produced by maghemitization. Ti/Fe ratio of this crystal is high (0.2–0.3) compared to other samples and rather close to that of commonly observed submarine basalts. The identification of titanomaghemite is quite difficult if only based upon Ti/Fe ratio obtained by the microprobe analyses without available standard samples. However, when the sample is scanned under microprobe analysis in comparison with a well-established standard maghemite specimen, we can safely identify not only the Ti/Fe ratio but oxygen/cation ratios with certainty. In the present case, the targeted crystal was identified as a maghemite under the optical microscope (as well as by microprobe analysis). This type of crystal was quite often observed in sample sections from Hole 538A.

Figure 5 shows titanomagnetites and ilmenite lamellae from Section 538A-35-4.

CONCLUSION

Magnetic characteristics of basement rocks of Hole 538A differ substantially from those commonly observed in submarine basalts. Microprobe analyses on the submarine basalts obtained showed x values around 0.6, which seems common for many other submarine basalts (Johnson and Hall, 1978). The x values can be calculated on a basis of $Ti^{+4}/(Fe^{+2} + Fe^{+3})$ ratio observed under microprobe. Usually titanomagnetite phases of these basalts show a certain degree of alteration (maghemitization). However, the Ti/Fe ratio should not largely deviate from the original value after low-temperature oxidation (i.e., empirically the deviation of the ratio after alteration is less than $\Delta x = \pm 0.05$). On the other hand, titanomagnetite with ilmenite exsolution lamellae often has a Curie temperature close to that of pure magnetite ($\sim 570°C$). The ilmenite lamella structures are believed to have been induced by some oxidation processes while the titanomagnetite crystals were still at high temperature shortly after eruption or intrusion of volcanic rocks. Therefore, we conclude that the coexisting titanomaghemite and ilmenite exsolution lamellae in the titanomagnetite crystals from Hole 538A imply two stages of oxidation: (1) high-temperature oxidation that was followed by (2) a series of low-temperature oxidations in a later stage after cessation of igneous activity (settlement of the volcanic formations).

ACKNOWLEDGMENTS

The authors would like to express sincere thanks to Drs. Nobuaki Niitsuma, Takatoshi Akimoto, and Margaret M. Testarmata for their valuable suggestions and critical reviews of this manuscript.

REFERENCE

Johnson, H. P., and Hall, J. M., 1978. A detailed rock magnetic and opaque mineralogy study of the basalts from the Nazca Plate. *Geophys. J. R. Astron. Soc.*, 52:45–64.

Date of Initial Receipt: July 7, 1982
Date of Acceptance: October 7, 1982

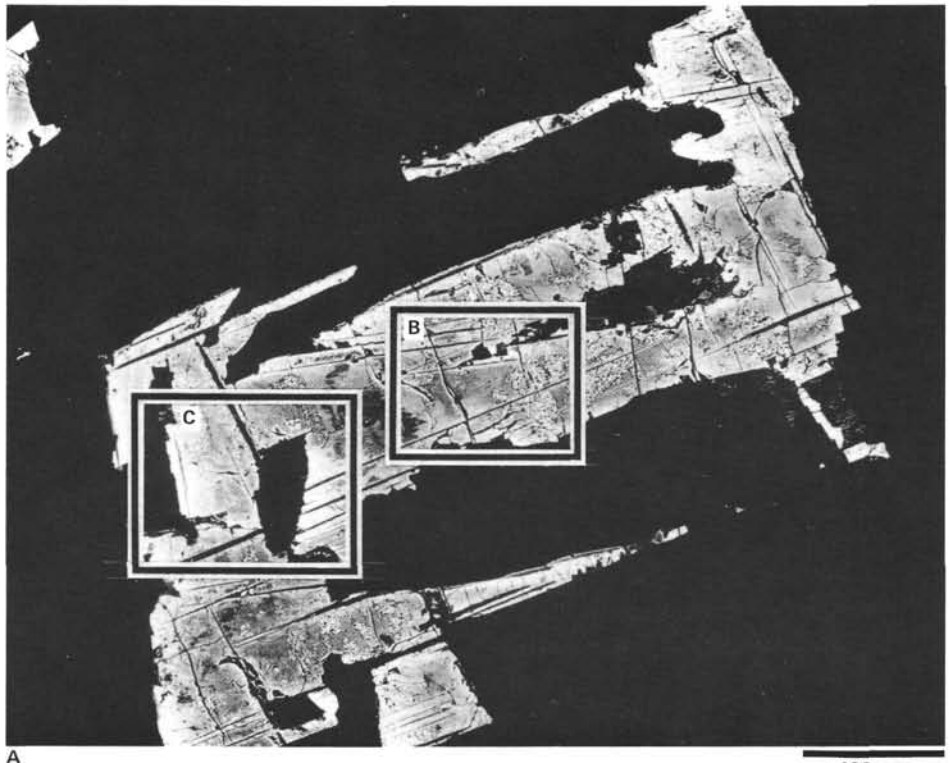

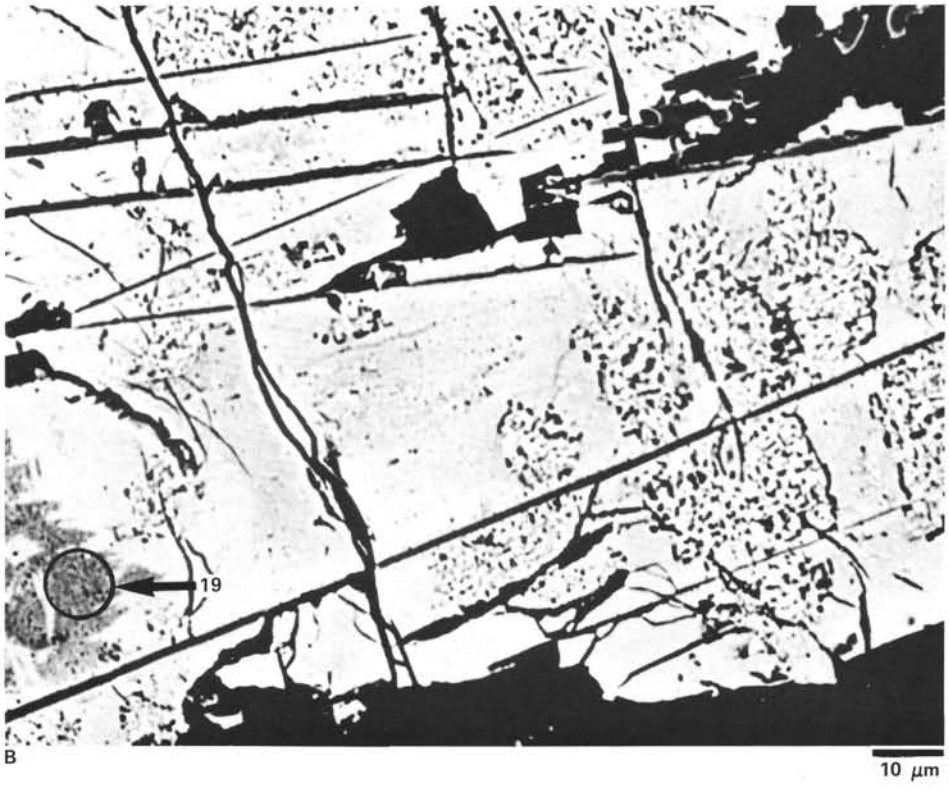

Figure 4. Microphotographs of electron compositional scanning image. The numbered arrows indicate analysis points (see Appendix B). A. Sample 538A-32-6, 77–79 cm; parts enclosed by squares labeled B and C correspond to Figures 4B and 4C. B. Enlarged part of Figure 4A. Straight ilmenite lamellae are seen. Analysis Point 19 suffered from low-temperature oxidation and was observed under a defocused beam. The x value around this point is 0.69. C. Enlarged part of Figure 4A; thick dark lamellae are ilmenites (Analysis Point 15). The bright part in this picture consists of titanomagnetite of moderate titanium content (Analysis Point 17).

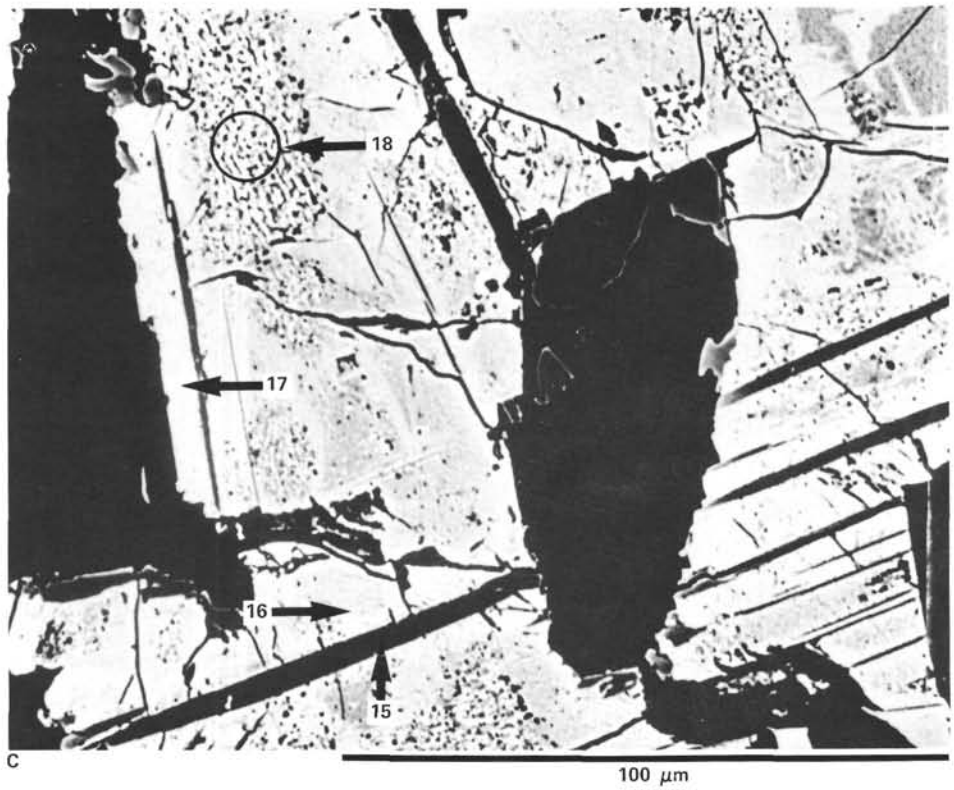

Figure 4. (Continued).

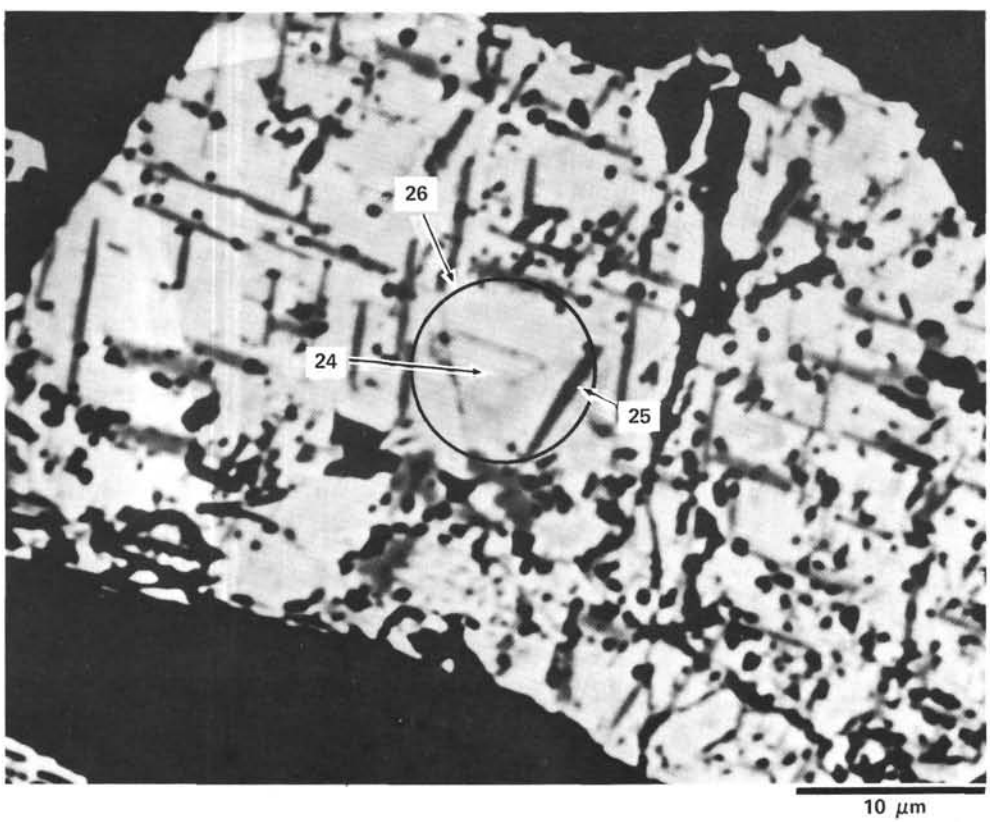

Figure 5. Section 538A-35-4; this sample consists of relatively small grains of titanomagnetites compared to those of Figures 3A and 4A. Ilmenite lamellae are highly developed and divided into small bands. A part of Analysis Point 25 consists of hemo-ilmenite composition.

APPENDIX A
Summary of Magnetic Properties, Hole 538A

Core-Section (interval in cm)	Jn (10^{-4}G)	k (10^{-3}G/Oe)	Js (emu/g)	Js-T[a] type	T_c (°C)	T_{ch}	J_h/J_o	Grain size (μ)	Rock	Remarks
30-1, 59-61	0.2	0.1	0.18	(R)	580	580	1.23	500	Gneiss	Ht rich
30-1, 135-137	0.2	0.2	0.62	I	570	590	3.01			
31-1, 18-20	5.9	2.5	2.37	(R)	580	565	0.89	50	Pl-cpx basalt	
31-1, 23-25	3.4*	2.1*	2.11	R	575	565	1.0	50	Pl-cpx basalt	
31-2, 47-50	0.1	0.1	0.07	I	555	575	1.20		Gneiss	
31-2, 125-128	0.3	0.1	0.17	R	570	570	1.01	10	Amphibolite	
32-1, 50-53	10.9	4.0	3.16	(R)	520	500	0.69	300	Pl-cpx dolerite	Sulfide rich
32-1, 119-121	9.5	2.9	3.03	(R)	550	535	0.93	500	Pl-cpx dolerite	Il-lamella
32-1, 132-134	9.9*	3.3*	2.49	(R)	550	530	0.94	300	Pl-cpx dolerite	
32-2, 50-53	8.7	3.8	2.68	(R)	550	525	0.92	250	Pl-cpx dolerite	Sulfide rich
32-2, 106-108	8.1*	3.1*	2.21	(R)	540	505	0.93	300	Pl-cpx dolerite	
32-2, 13-136	6.7	3.7	2.87	(R)	555	530	0.93	250	Pl-cpx dolerite	Sulfide rich
32-3, 29-31	4.2	3.5	3.62	(R)	545	525	0.91	400	Pl-cpx dolerite	Il-lamella
32-3, 70-72	6.4*	3.2*	3.07	(R)	560	545	0.97	300	Pl-cpx dolerite	Il-lamella
32-4, 16-18	10.9*	3.3*	2.16	(R)	555	535	0.97	250	Pl-cpx dolerite	
32-4, 54-56	2.7	3.6	2.73	(R)	565	550	0.95	300	Pl-cpx dolerite	Sulfide rich
32-5, 33-35	6.9*	3.0*	2.07	(R)	550	535	1.04	500	Pl-cpx dolerite	Il-lamella
32-5, 39-41	16.0	3.8	2.39	R	570	565	1.0	400	Pl-cpx dolerite	Il-lamella
32-6, 109-111	7.4	3.8	3.14	(R)	530	510	0.90	300	Pl-cpx dolerite	Il-lamella
32-6, 77-79	6.8*	3.5*	2.36	(R)	525	505	0.87	400	Pl-cpx dolerite	Il-lamella
33-1, 88-90	1.0	3.4	3.33	R	570	560	1.0	100	Amphibolite	High altered Mt
33-2, 81-83	0.1*	0.1*	0.09	(R)	550	550	1.84	80	Amphibolite	High altered Mt
33-2, 99-101	0.1	0.1	0.09	I	210	550	1.84	60	Amphibolite	High altered Mt
34-1, 50-53			0.16	R	535	530	1.0	100	Amphibolite	Il and Ht rich
35-1, 14-16	5.3*	1.1*	1.39	R	550	545	1.13	60	Pl-cpx basalt	Il and Ht rich
35-1, 106-108	20.4	4.7	3.88	(R)	550	550	0.92	200	Pl-cpx dolerite	Sulfide rich
35-2, 109-111	14.8	4.5	3.83	R	550	535	0.96	500	Pl-cpx basalt	Sulfide rich
35-3, 10-13			0.23	R	570	565	1.10	500	Pl-cpx dolerite	Sulfide rich
35-3, 146-148	18.4*	3.2*	5.55	(R)	550	530	0.91	500	Pl-cpx dolerite	
35-4, 69-71	11.5	2.8	0.62	R	560	550	0.96	200	Pl-cpx dolerite	
35-4, 94-96	33.9*	3.7*	4.45	R	550	535	0.93	150	Pl-cpx dolerite	Il-lamella
36-1, 50-53	7.8	4.8	0.47	(R)	550	525	0.91	300	Pl-cpx dolerite	Sulfide-rich
36-1, 89-91	20.2*	4.1*	5.72	(R)	550	525	0.90	150	Pl-cpx dolerite	Very highly altered
36-1, 109-111	10.6	3.7	4.02	(R)	545	530	0.94	150	Pl-cpx dolerite	
36-2, 86-88	7.5*	3.8*	3.03	R	595	590	1.03	150	Pl-cpx dolerite	Il rich
36-3, 21-23	2.5*	1.1*	1.62	R	580	575	1.10	200	Pl-cpx dolerite	Il-lamella
36-3, 39-41	<0.1	<0.1	0.08	R?	580?	680?	1.1		Ol websterite	Il only

Note: Jn = natural remanent magnetization; k = susceptibility; Js = saturation magnetization; Js-T = temperature dependence of Js; R = reversible; I = irreversible; parentheses indicate atypical curves; T_c = Curie temperature observed during heating; T_{ch} = Curie temperature observed during cooling; J_h/J_o = the ratio of saturation magnetization observed at room temperature after and before heating; Pl-cpx = plagioclase and clinopyroxene phenocrysts; Ol = olivine phenocryst; Ht = hematite; Mt = magnetite; Il = ilmenite. Asterisks denote shipboard measurements. ? means that, because the magnetic moment of this sample is very weak, we could not precisely determine the type or temperature.

APPENDIX B
Chemical Composition of Opaque Minerals in Hole 538A Dolerites

Analysis point number	SiO_2	TiO_2	Al_2O_3	FeO[a]	MgO	MnO	NiO	V_2O_3	Cr_2O_3	Total	Ti/Fe (atomic mole ratio)	x value[b]
Sample 538A-32-1, 119–121 cm												
1	2.76	0.89	0.34	89.52	0.16	0.09			0.01	93.77	0.001	0.027
2	1.86	1.77	0.40	89.50	0.14	0.14			0.01	93.82	0.006	0.019
3	0.94	10.30	1.20	80.97	0.10	0.10	0.05	0.53	0.03	94.22	0.114	0.308
4	0.73	23.63	0.46	71.61	0.23	0.39	0.04	0.54	0.05	97.22	0.297	
5	1.32	12.60	0.63	79.91	0.07		0.07	0.54	0.01	95.15	0.142	0.373
6	3.93	21.51	0.80	63.68	0.84	0.07	0.05	0.54	0.03	91.45	0.304	0.699
7	0.16	46.91	0.13	50.51	0.49	1.03		0.30	0.02	99.25	0.835	
8	0.15	7.67	1.82	86.63	0.11	0.25		0.60	0.01	97.24	0.080	0.221
9	0.10	46.07	0.15	51.48	0.48	1.22	0.01	0.30	0.02	99.83	0.805	
10	0.14	46.58	0.11	49.64	0.54	1.08	0.03	0.32	0.02	99.46	0.880	
Sample 538A-32-6, 77–79 cm												
11	0.16	19.74	1.48	72.29		1.50	0.03	0.74	0.03	95.97	0.246	0.592
12	0.17	21.84	1.58	69.13	0.50	0.44		0.80	0.02	94.48	0.284	0.664
13	1.55	20.69	1.68	69.40	0.17	0.47	0.03	0.72	0.01	94.72	0.268	0.634
14	0.18	21.43	1.82	70.94	0.03	1.76	0.02	0.60	0.03	96.81	0.272	0.641
15	0.13	51.59	0.05	48.37	0.55	0.83		0.26	0.01	101.79	0.959	
16	0.16	19.98	0.98	73.14	0.02	0.94		0.51	0.02	95.75	0.246	0.592
17	0.11	16.36	0.68	77.02		1.21	0.02	0.47		95.87	0.191	0.481
18	0.06	20.84	0.64	74.36	0.20	0.46		0.39		96.95	0.252	0.604
19	0.17	23.01	1.09	69.34	0.06	0.60		0.50	0.01	94.78	0.299	0.690
Sample 538A-35-4, 94–96 cm												
21	0.15	19.35	1.67	71.69	0.28	0.91		0.41	0.04	94.50	0.243	0.586
22	0.17	8.77	1.64	81.57		0.35		0.72	0.04	93.26	0.097	0.265
23	0.40	25.74	1.01	64.77	0.02	1.57	0.01	0.55	0.05	94.12	0.357	
24	0.50	12.01	1.14	78.82	0.03	0.27		1.11	0.03	93.91	0.137	0.362
25	0.33	38.91	0.42	54.89	0.06	2.49		0.55		97.65	0.637	
26	0.73	19.36	1.55	70.71	0.25	0.94	0.03	0.67	0.04	94.28	0.246	0.593

Note: Blanks indicate that the compound was not detected.
[a] Total iron as FeO.
[b] Value in the formula $x\ Fe_2\ TiO_4 \cdot (x - 1)\ Fe_3O_4$.